

Article

Some Aspects of Oxidation and Reduction Processes in Ti–Al and Ti–Al–Nb Systems

Marzena Mitoraj-Królikowska *  and Ewa Drożdż 

Inorganic Chemistry Department, Faculty of Materials Science and Ceramics, AGH University of Science and Technology, Al. Mickiewicza 30, 30-059 Krakow, Poland; edrozd@agh.edu.pl

* Correspondence: mmitoraj@agh.edu.pl

Abstract: The oxidation of titanium and titanium aluminides has attracted the attention of scientists for many years because of their high-temperature application. The most popular method to investigate oxidation behavior is the measurement of alloy mass changes during exposure to elevated-temperature under isothermal or thermal cycling conditions. However, the thermogravimetric method is not enough to establish an oxidation mechanism. In this paper, the temperature-programmed oxidation (TPOx) and reduction (TPR) were applied for the Ti–Al and Ti–Al–Nb systems, which was a new experimental concept which revealed interesting phenomena. Although oxidation of titanium alloys is well-described in the literature, not many papers present at the same time reduction of oxidized alloys. The results presented in the paper concentrated on the first stages of oxidation, which are scarcely described in the literature, but are important to understand the oxidation mechanism. Comparison between powder and bulk samples with similar compositions revealed essential differences in the oxidation mechanism.

Keywords: titanium; titanium aluminides; TNB; oxidation; reduction



Citation: Mitoraj-Królikowska, M.; Drożdż, E. Some Aspects of Oxidation and Reduction Processes in Ti–Al and Ti–Al–Nb Systems. *Materials* **2022**, *15*, 1640. <https://doi.org/10.3390/ma15051640>

Academic Editor: Stefano Lettieri

Received: 24 January 2022

Accepted: 18 February 2022

Published: 22 February 2022

Publisher's Note: MDPI stays neutral with regard to jurisdictional claims in published maps and institutional affiliations.



Copyright: © 2022 by the authors. Licensee MDPI, Basel, Switzerland. This article is an open access article distributed under the terms and conditions of the Creative Commons Attribution (CC BY) license (<https://creativecommons.org/licenses/by/4.0/>).

1. Introduction

There is a lot of information in the literature on the oxidation of titanium and titanium aluminides alloys at various temperatures. Generally, the titanium oxidation reaction is described as the result of two processes: diffusion of oxygen into the bulk of the sample and desorption of O atoms from the surface with concomitant reduction of the Ti oxidation state. The diffusion process is stimulated by temperature increase, however at the same time, as the temperature is rising significantly, the process of oxygen desorption becomes more intense. Moreover, it is known that high-temperature treatment promotes the mobility of oxygen in the oxide lattice. In general, the mentioned processes are controlled mainly by the duration of exposure to O₂ and the temperature of the samples. According to Lu et al. [1] these two opposing trends indicate 227–327 °C as the optimal temperature-range for maximum oxidation of titanium. Furthermore, titanium at room-temperature (RT) oxidizes at the very beginning of oxygen exposure, and the only oxide recognized at RT is TiO₂. The oxidation at a higher-temperature is different and is determined by oxygen solubility [2]. The maximum solubility of oxygen in alpha titanium according to the concentration profile for the solid solution of Ti (O) is equal to 34 at.% [3] and is a function of temperature and time. Maximum solubility could be achieved in relatively short time at the temperature above 760 °C [4]. The composition of titanium compounds depends on time and temperature. The rutile phase (TiO₂) is present in the oxidation products in all temperature-ranges [5]. At a higher-temperature, traces of other oxides, such as Ti₂O₃ (above 650 °C) [5], TiO, and Ti₃O₅ (above 800 °C) [6], were also detected. Generally, under the uniform and compact TiO₂ layer, internal, rather loose, lower titanium oxides are present [6].

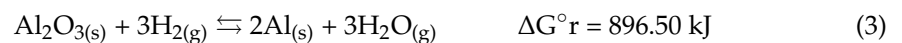
Hydrogen reduction of TiO₂ is an important and promising reaction for the production of environmentally friendly titanium powder. Currently, on an industrial scale the energy-consuming Kroll method is used. Theoretically, from the thermodynamic point of view, reduction of TiO₂ has positive and negative Gibbs Free Energy value depending on the form of hydrogen:



The above values were determined at temperature 25 °C on the basis of data from the NIST database [7].

The aluminum oxidation at the RT is exothermic (by 3.6 kcal/mol) and the reaction mechanism is not very simple, what was predicted on the basis of the theoretical calculations by Marshall et al. [8]. Garland [9] experimentally confirmed that the reaction of Al + O₂ in the temperature and pressure range: 25–827 °C and 0.01–0.13 atm, respectively, proceeds by transfer of O[−] ions in two main stages: formation of the OAlO complex and decomposition of this complex to AlO + O. These stages are rarely mentioned by the authors and most of them stated that the reaction of aluminum with oxygen below 400 °C does not proceed to the crystalline phase (only a thin amorphous layer is formed) and only above this temperature this layer crystallizes: first into γ-Al₂O₃ phase, next with the increase in the temperature to θ-Al₂O₃ and then α-Al₂O₃ phase appears [10].

The idea of Al₂O₃ reduction with hydrogen is not very new but the reduction mechanism is still not well recognized. Similarly, like for TiO₂, Gibbs Free Energy is only negative for atomic hydrogen:



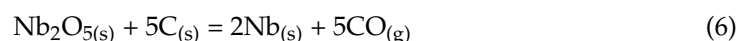
The above values were determined at temperature 25 °C on the basis of data from the NIST database [7].

Niobium has a high affinity for oxygen and in the niobium–oxygen system, the niobium element can be found in four different oxidation states: 0, 2⁺, 4⁺, and 5⁺, generally related to the phases of metallic Nb and to the NbO, NbO₂, and Nb₂O₅, respectively [11]. According to Delheusy et al. [12], it is a triple layer consisting of NbO, NbO₂, and Nb₂O₅. Nico et al. [13] reported that during annealing of niobium in the air atmosphere (from room-temperature to about 1000 °C) the formation of cubic NbO in the temperature-range of 100–370 °C can be observed, around 300 °C the amorphous phase appears and again, approximately 500 °C, a crystalline phase of niobium (V) oxide is created. In addition, the first orthorhombic phase was detected, while the monoclinic phase at around 850 °C also appeared. In the same article, the authors suggested that two exothermic peaks on the DTA curve between 300 and 500 °C correspond to the oxidation of NbO (the first peak) and the crystallization of Nb₂O₅ from amorphous phase (the second one).

The reduction of Nb₂O₅ reduction is a basic process in niobium production. The most of niobium obtained from the reduction of niobium pentoxide is produced with aluminothermic reaction:



Sometimes the carbothermic two-stage process is used for niobium production with the overall reduction reaction:



Reduction of Nb_2O_5 with hydrogen is rarely described in the literature. According to the basic experiments [14], niobium pentoxide was readily reduced to tetroxide, but further reduction was rather slow.

The use of titanium alloys that contain aluminum and other alloying elements in the automotive and transport industries is often due to the strict requirements related to the high oxidation resistance of materials for such applications. As a result of high-temperature oxidation of these alloys, mainly the formation of Al_2O_3 and TiO_2 oxides is observed. According to the binary Ti–Al phase diagram [15] when the concentration of aluminum in titanium is greater than 20 at.% formation of titanium aluminides intermetallic phases is observed. Titanium aluminides phases were predicted as a lightweight and oxidation resistant alloys for special applications in the automotive and airline industry. The first generation of these alloys was based on γ -TiAl phase (gamma alloy). Because of the high aluminum concentration, the oxidation resistance of the gamma alloy was better than that of titanium. However, depending on the oxygen pressure and metal activity, either Ti or Al may oxidize preferentially. The products of oxidation are rutile (TiO_2) and α -alumina (Al_2O_3). Compared to alumina, titania has a high diffusivity of oxygen and poor protectiveness that result in a reduced oxidation resistance of the γ -TiAl alloy especially at temperatures exceeding 800 °C.

The second generation of titanium aluminides alloys was represented by advanced ternary and quaternary alloys: Ti-(45-48)Al-(1-3)Cr, Mn-(2-5)Nb, Ta, Mo in at.% [16]. The third generation of the Nb- rich alloys with general composition: Ti-(45-46)Al-(5-10)Nb-(0-0.5)B, C in at.% termed as TNB alloys were developed to improve room-temperature ductility and high-temperature creep resistance [17,18]. Titanium aluminides with 45–46% of aluminum are based on two phases: γ -TiAl (85–92 vol.%) and α_2 - Ti_3Al (8–15 vol.%) and have mainly lamellar microstructure [19]. It was also found that Nb as a slow diffuser in the Ti–Al system influences the oxidation of these alloys; however, the exact mechanism of oxidation in the presence of Nb has not yet been found [20]. Different hypotheses are described in the literature. Some authors believe that the Nb cation with valence 5^+ , when incorporated into TiO_2 (usually nonstoichiometric with composition TiO_{2-x} , where X is about 0.02) substitutes for the Ti^{4+} cation and reduces oxygen vacancies in TiO_2 and this results in decreased oxygen diffusion and consequently reduction in the growth of TiO_2 . Another explanation of Nb influence is enhancement of Al_2O_3 formation [21]. It is worth mentioning that the addition of niobium can also improve the oxidation resistance of titanium alloys with a lower aluminum content [22].

The aim of this work was to compare and investigate oxidation/reduction processes in Ti–Al and Ti–Al–Nb systems (for powders and solid materials) on the basis of temperature-programmed oxidation (TPOx) and reduction (TPR) measurements completed with X-ray diffraction analysis. The work was motivated by an attempt to better understand the oxidation of the Ti–Al–Nb alloy, as well as to recognize the reduction of titanium-based materials in the context of their catalytic behavior [23] and the future application in contact with hydrogen fuel.

2. Materials and Methods

The powder and solid materials were used for experiment. In the case of powder samples, the following commercially available materials were used: Al—aluminum powder (99.8%, about 45 μm , SunChemical, Parsippany-Troy Hills, NJ, USA); Ti—titanium powder (>98.0%, about 150 μm , Merck, Darmstadt, Germany); Nb—niobium powder (99.8%, 45 μm , Sigma Aldrich, Saint Louis, MO, USA); and Ti–Al—titanium aluminides powder (with composition: Ti–50Al in at.%, after SHS synthesis and ball milled to the grain size about 90 μm). For comparison, five solid samples were examined: Al—aluminum (electrolytic); Ti—titanium (99.6%, Goodfellow, Huntingdon, England); Nb—(99.9%, PolAura, Zabrze, Poland); Ti–Al—titanium aluminides (with composition: Ti–50Al in at.%, arc-melted powder previously mentioned powder); and Ti–Al–Nb—TNB titanium aluminides (with composition: Ti–46Al–8Nb in at.%, produced by Access e.V.,

Aachen, Germany with fully lamellar microstructure). Samples in the form of cuboids and cylinders (niobium) with an area of 50–70 mm² and weight of about 0.1–0.2 g before measurements were ground with emery papers up to P1200 (ISO/FEPA) and rinsed with distilled water.

TPOx and TPR measurements were conducted on ChemiSorb 2750 apparatus (Micromeritics Instrument Corporation, Norcross, GA, USA) in the flow of 2% O₂/Ar and 5% H₂/Ar mixtures, respectively. The samples (powders/solids) were placed in a quartz reactor and after flushing the system with helium it was heated at a rate of 10 deg/min. The masses of samples used in tests were around 0.6–0.7 g for powders and around 0.1–0.2 g for solids. The materials were first oxidized (TPOx) and then reduced (TPR). The TPR/TPOx measurements were normalized with respect to the mass of the samples (to 1 gram of sample mass), due to the fact that no materials of identical mass were used for the measurements.

Powder and solid samples after TPOx or TPR measurement were examined with a scanning electron microscope (SEM) (Nova Nano SEM 200 FEI Company, Hillsboro, OR, USA) using secondary or backscattered electron images (SEI or BEI). The chemical and phase composition of the samples were determined by energy-dispersive X-ray spectroscopy (EDS) (EDAX, AMETEK, Inc., Berwyn, IL, USA) and X-ray diffraction (XRD) (Seifert XRD7, XRD Eigenmann GmbH, Felsenweg, Germany), respectively. Some of the solid samples were selected for the preparation of metallographic cross-sections. For this purpose, the samples were embedded in epoxy resin and polished with water-based diamond suspensions (grain size: 9, 3, and 1 μm).

3. Results and Discussion

3.1. Oxidation and Reduction of Powders

In Figure 1, TPOx results precede TPR measurements. As can be seen in the case of the TPOx profile for Ti, a slight effect related to oxygen consumption around 230 °C appears, however only ca. 400 °C the actual process begins. During the process, the consumption of oxygen is so rapid that "oxygen starvation" is observed after a few minutes. Nevertheless, on the basis of the presented TPOx profile, it can be concluded that the oxidation of titanium is a complex process, probably associated with the formation of at least two types of oxide.

Inhibition of the reaction related to oxygen deficiency can additionally affect the oxidation mechanism, increasing the likelihood of the formation of titanium oxides at a lower oxidation state. Since the observations of the color of oxides are often closely related to their phase composition, the figure below shows digital pictures of the quartz reactor (used for the TPOx/TPR test) with the powder after oxidation (Figure 2a). One can notice that the colors of Ti powder after oxidation are diverse.

According to the XRD analysis shown in Figure 3a, the predominant phases for the oxidized titanium powder were Ti₃O (hexagonal) and TiO₂ (rutile). The titanium-richer phase (Ti₃O) was most likely formed due to the insufficient amount of oxygen during TPOx. During oxidation, oxygen can dissolve in the octahedral interstices of titanium lattice up to 34 at.%. and occupied half of the available interstitial sites, and, therefore, the limiting composition is Ti₂O. The Ti₃O structure consists of a closed-packed hexagonal arrangement of titanium atoms with every second layer of octahedral interstices normal to the c-axis vacant. One-third of the oxygen sites in the occupied layers are empty and these vacancies have an ordered arrangement in the direction of the c-axis [24]. It is worth noting that the XRD results presented in Figure 3 were obtained from the powder mixture visible in the quartz reactor after oxidation (a) and after reduction (b), respectively.

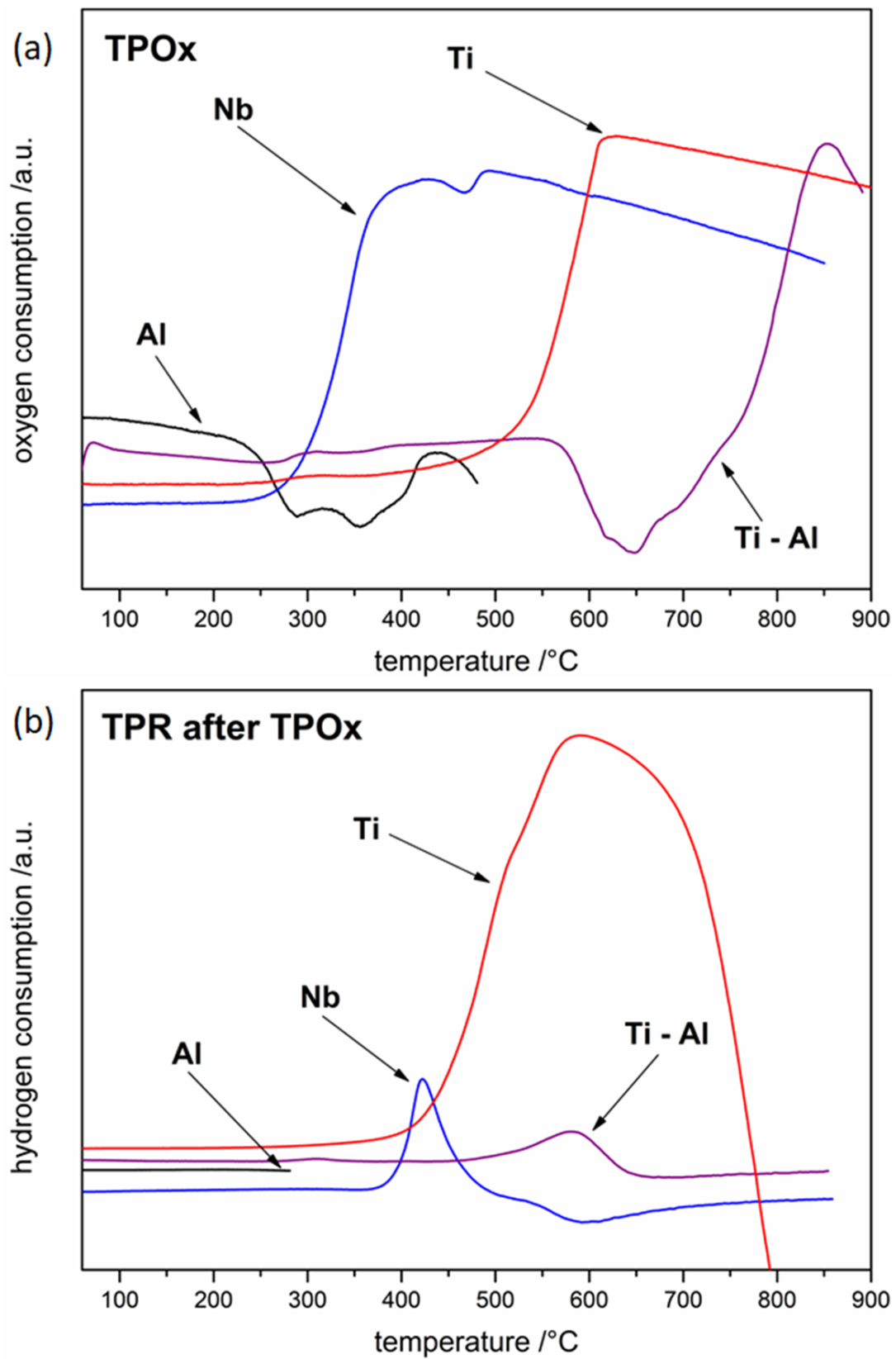


Figure 1. The oxidation (a) and reduction (b) profiles of tested powders.

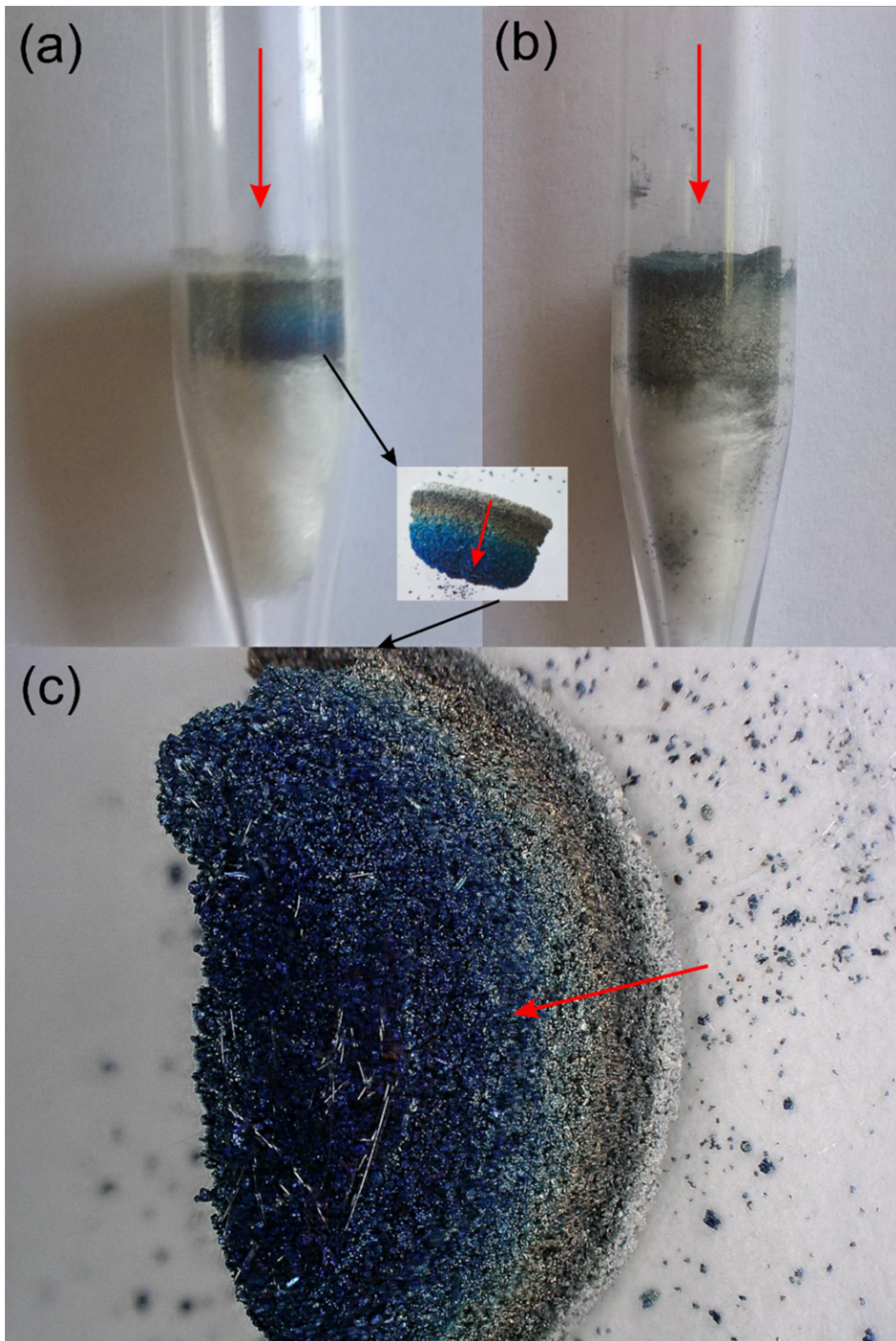


Figure 2. Quartz reactor with Ti powder after TPOx (a), and after TPOx + TPR (b) and a higher-magnification of oxidized powder (c). Arrows indicate the flow direction of the O₂/Ar or H₂/Ar mixture.

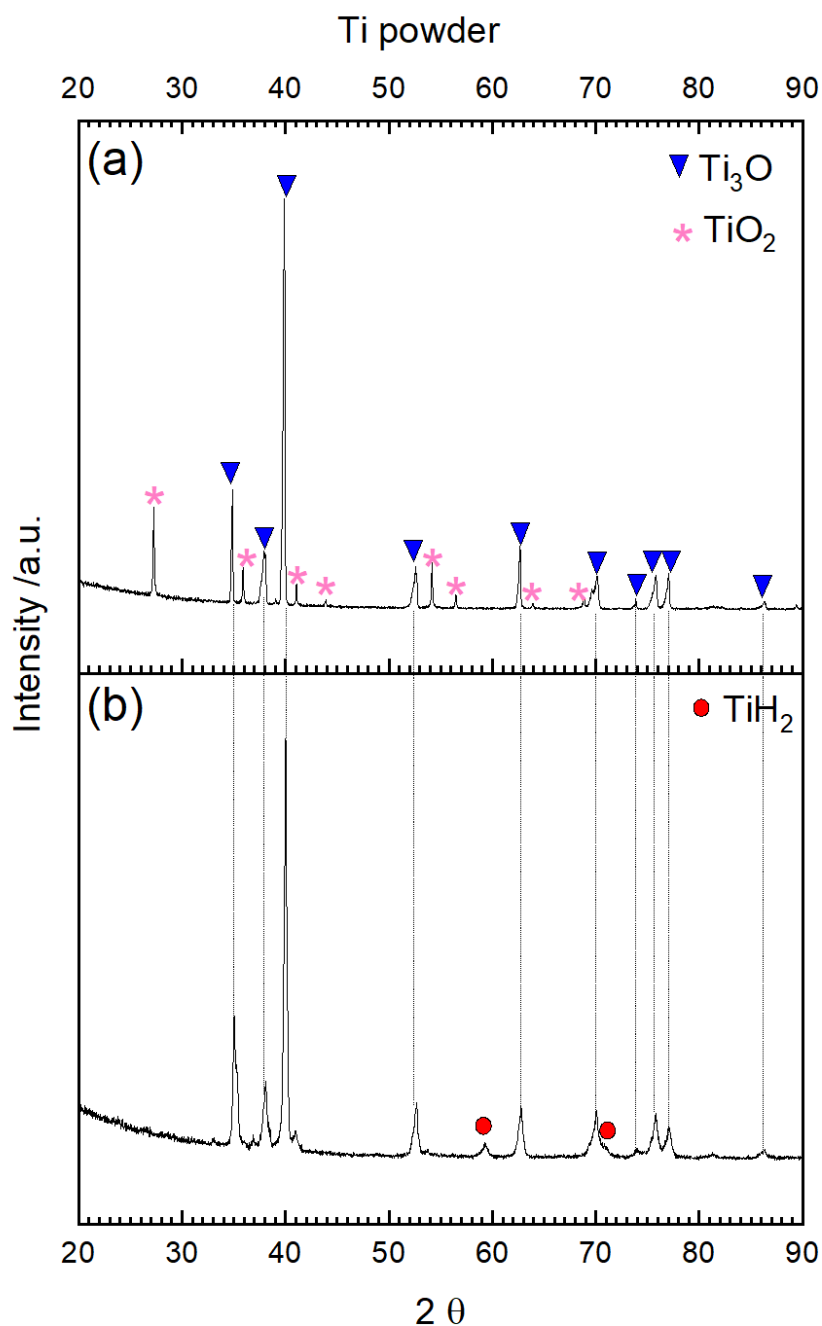


Figure 3. XRD diffraction pattern of Ti powder after TPOx (a) and after TPOx + TPR (b).

The colors visible in the reactor after TPOx in the digital picture shown in Figure 2a,c can be an effect of the presence of various oxide species, as well as TiO_2 non-stoichiometry. It is also interesting to mention that different titanium oxides can have different colors: TiO_2 is white, TiO has a brown-goldish color, Ti_3O_5 is bluish, and Ti_2O_3 is dark violet [25]. Different colors were also found for defective TiO_2 , for example due to the intentional introduction of oxygen vacancies as a kind of self-doping. For example, blue TiO_2 was synthesized by incorporating Ti^{3+} derived from the TiCl_3 precursor directly into the TiO_2 matrix [26]. Blue hydrogenated rutile TiO_2 was also obtained through the high-temperature and high-pressure hydrogen reduction of white rutile. The blue color of TiO_2 is commonly ascribed to oxygen vacancy, surface disorder, and oxygen deficiency [27]. The yellow color of TiO_2 was an effect of Nb doping by ultrasonic spray pyrolysis of the aqueous peroxide precursor solution. Nb^{5+} and Ti^{3+} ions were responsible for coloration [28].

Yellow color of TiO_2 was also achieved without any dopants by the titanium vacancies (acceptor) and titanium interstitials (donor) that incorporated in the TiO_2 by simple UV light assisted sol–gel method [29]. Different colors of titanium oxides were also identified during the controlled transformation of Ti_2O_5 to anatase/rutile TiO_2 under oxidizing conditions. The color of the annealed particles progressively changed from black (25 °C) to dark green (500 °C), orange (600 °C), yellow (700 °C), and white (≥ 800 °C). The orange and yellow powder after annealing at 600 and 700 °C, should be the rutile TiO_2 with oxygen vacancies [30]. The XRD analysis in Figure 3a does not confirm the presence of these oxides, suggesting that the visible colors are due to the nonstoichiometry of TiO_2 or that the amounts of residual oxides are below the detection limit of the XRD method.

The TPR profile for titanium (Figure 1b) indicated, that titanium is first reduced (slow onset around 250 °C); however, the actual process occurred at approximately 350 °C. The mechanism of rutile reduction was described in detail by Khader et al. [31]. According to V. Bratan et al. [32], who reported the results of the temperature-programmed reduction measurement (with heating rate of 10 deg/min in a stream of 5% H_2/Ar), the reduction of TiO_2 starts already above 340 °C. The TPR profile for Ti is complex (several maxima), which proves that several reduction processes occur. This can be a confirmation of the presence of several different oxide species formed during oxidation or this can be an effect of possible gradual reduction of TiO_2 through the lower oxides. Moreover, one can notice that the TPR line at around 800 °C decreases sharply below the baseline, which indicates a rapid release of hydrogen by the system. This effect corresponds to the decomposition of titanium hydride TiH_2 , which was formed at a lower-temperature by the direct reaction of titanium with hydrogen. TiH_2 is stable up to around 150 °C and above this temperature decomposes. It is interesting to note that reduction of TiO_2 is described in the literature as difficult process and rather strong reducing atmospheres were used, for example hydrogen plasma [33] or metal-hydride-reduction process (MHR) [34] in order to reduce TiO_2 only partially to Ti_3O_5 , Ti_2O_3 , or TiO . Theoretically, the reduction of TiO_2 according to the phase diagram [35] should give the following oxides: TiO_{2n-1} (so-called Magneli phases), Ti_3O_5 , Ti_2O_3 , TiO , Ti_3O_2 , Ti_2O , and Ti_3O , but rarely this sequence is followed. There is one possible explanation. Water vapor, which is a by-product of reduction reactions, would cause the reverse re-oxidation. It was also found [33] that a thinner TiO_2 oxide is more difficult to reduce than a thicker one, which was, for example, explained with a high affinity of titanium for hydrogen. Indeed, it is well known that Ti easily reacts with hydrogen with TiH_2 formation [36] which is another limiting factor for direct TiO_2 to Ti reduction.

The diffraction analysis for titanium powder after TPOx–TPR cycles (Figure 3b) indicates that the reflections of the TiO_2 phase almost disappeared, and Ti_3O becomes the main phase. It seems that during the TPR cycle the highest Ti oxide (TiO_2) was reduced to the lowest (Ti_3O), possibly through the intermediate oxides, which were totally reduced at the end of TPR. At the same time, the color of the powder changed to dark gray (Figure 2b). The presence of the remaining, undecomposed TiH_2 was also confirmed with XRD analysis (Figure 3b), which is in agreement with the described TPR curve.

Interestingly, in the case of the TPOx line for aluminum, an effect opposite to oxygen consumption was observed at a temperature of about 200 °C (Figure 1a). The complexity of the TPOx profile proves that oxidation is at least a two-stage process. It seems that the most likely explanation of this effect is the aforementioned (referenced in the Introduction) decomposition of the OAlO complex formed in the first stage of aluminum oxidation to AlO with oxygen released simultaneously (to the atmosphere above the sample).

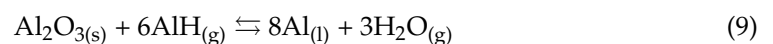
The oxidation of aluminum powder was problematic due to the low melting-point (660.3 °C) and the fast sublimation of Al particles. The XRD pattern of oxidized aluminum powder did not confirm the presence of oxide (Al_2O_3). This observation is consistent with the literature where amorphous Al_2O_3 is featured [37,38]. In the case of aluminum powder oxidation, amorphous Al_2O_3 is thermodynamically more stable than the crystalline form. The amorphous Al_2O_3 oxide is very thin, and its growth is controlled by the outward diffusion of aluminum cations that prevents crystallization of the oxide. Moreover, the

further oxidation of aluminum is limited because of well-known protective properties of Al_2O_3 [39]. At the temperature higher than $300\text{ }^\circ\text{C}$, the amorphous Al_2O_3 layer reaches the critical thickness which ranges between 0.5 nm and 4 nm depending on the study [40,41] and after that crystalline $\gamma\text{-Al}_2\text{O}_3$ begin to form. Around the temperature $800\text{ }^\circ\text{C}$, the $\gamma\text{-Al}_2\text{O}_3/\theta\text{-Al}_2\text{O}_3$ scale is stable. In the temperature-range $850\text{--}1100\text{ }^\circ\text{C}$, $\theta\text{-Al}_2\text{O}_3$ transforms to $\alpha\text{-Al}_2\text{O}_3$ [42,43]. Even at the temperature $1400\text{ }^\circ\text{C}$, the complete oxidation of the aluminum powder did not take place [43].

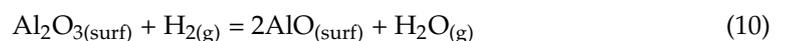
Aluminum powder reduction was not carried out to very high-temperatures due to the possibility of aluminum evaporation. Al_2O_3 in contact with aluminum can be reduced according to the reaction written in the introduction part to the aluminum nano-powder, which can very easily evaporate. It was also possible that nanosized aluminum from the reduction of Al_2O_3 can further react with hydrogen with the formation of aluminum hydride (AlH_3), which can then very-readily decompose. According to the phase diagram calculated from Barin and Knacke data [44], aluminum from alumina can be obtained at a temperature much higher than the melting-point of aluminum, and, at the same time, the partial pressure of the water vapor should be kept very low [45]. On the other hand, hydrogen can dissolve in molten aluminum and the amount of dissolved hydrogen can be calculated with the empirical equation [46]:

$$\log(S/S^\circ) - 1/2\log(p/p^\circ) = (-2700/T) + 2 \cdot 72 \quad (7)$$

where: S° is a standard value of solubility equal to 1 cm^3 of diatomic hydrogen measured at $0\text{ }^\circ\text{C}$ and 101325 Pa (1 atm) per 100 g of metal, p° is a standard pressure equal to 101325 Pa (1 atm), and T is absolute temperature. It is generally accepted that hydrogen is dissociated into the atomic state when dissolved in aluminum which can explain possibility of alumina reduction when alumina is in contact with molten aluminum. A certain amount of molecular hydrogen is probably also present in hydrogen gas [45]. It was experimentally confirmed [45] that it is possible to reduce alumina with hydrogen to aluminum when molten aluminum is present in the system. However, at the same time competitive reaction can take place:



At the temperature below the melting-point of aluminum ($450\text{--}550\text{ }^\circ\text{C}$) nonstoichiometric black alumina ($\text{Al}_2\text{O}_{2.908}$) was detected after hydrogen reduction [47]. The amount of nonstoichiometric alumina was consistent with possible surface reduction:



In the case of the Ti–Al powder alloy, the TPOx profile in the temperature-range $550\text{--}750\text{ }^\circ\text{C}$ is similar to the aluminum profile in the temperature-range $230\text{--}430\text{ }^\circ\text{C}$, as can be seen in Figure 1a. Therefore, it can be concluded that the decomposition of the OAlO complex for Ti–Al powder is visible at a temperature around $300\text{ }^\circ\text{C}$ higher than for pure aluminum powder. Furthermore, it is worth noting that around $270\text{ }^\circ\text{C}$ slight oxygen consumption begins, which can confirm the formation of the Al_2O_3 oxide layer. However, it seems that the oxide layer was very thin or amorphous because in the case of Ti–Al powder after TPOx conducted up to $530\text{ }^\circ\text{C}$ and intentionally interrupted for XRD analysis (not presented here) oxides were not detected. The only recognized phases according to XRD came from the substrate powder: Ti–Al (the main phase) and Ti_3Al (the minor phase).

Additionally, as shown in Figure 1a on the Ti–Al powder TPOx profile, around $750\text{ }^\circ\text{C}$ the main oxidation process begins, which is probably connected with titanium oxidation, since the shape of the TPOx profile is very similar to this measured for titanium powder but at around $300\text{ }^\circ\text{C}$ lower-temperature. The results obtained for the Ti–Al powder confirmed the higher oxidation resistance of the Ti–Al alloys described in the literature compared to those of pure titanium and aluminum.

The TPR profile for Ti–Al powder after TPOx shows the maximum shifted to the higher-temperature (beginning around 460 °C) in comparison to the maximum that appeared for titanium reduction. The effect is small compared to that seen for pure titanium.

It is worth noting that in the case of oxidation and reduction of Ti–Al material on TPOx/TPR profiles, slight effects related to the reaction occur, while the phase composition determined on the basis of XRD measurements does not change. This fact proves that the TPOx/TPR method is much more sensitive compared to the XRD method.

Analysis of the behavior of the niobium powder sample during thermal heating in oxidizing atmosphere shows that the first oxidation effect appears for Nb at about 220 °C (Figure 1a). The shape of the TPOx profile in Figure 1a corresponding to the oxidation of niobium proves that it is a quite rapid process which consists of at least three stages. The first peak (composed of two maxima at 380 and 430 °C) probably corresponds to oxidation of niobium to lower oxides, the next effect (at about 460 °C) is inhibition of the oxidation process, and the last one is the next peak corresponding to the oxidation process. From around 480 °C, a decrease in the TPOx line, characteristic of the so-called “oxygen starvation”, can be seen similar to the effect for titanium powder.

The three stages of oxidation visible in the TPOx line for niobium correspond to the three layers of niobium oxide reported in [12] and with the three main layers of niobium powder visible in the digital picture of the reactor in Figure 4a. All the visible layers of powder were analyzed with XRD separately.

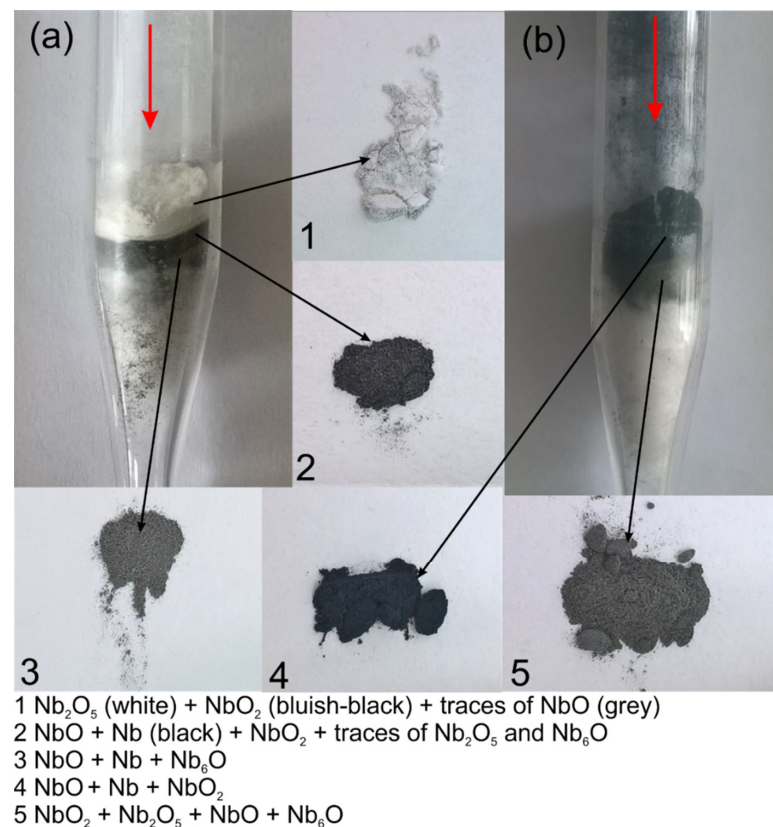


Figure 4. Quartz reactor with Nb powder after TPOx (a) and after TPOx + TPR (b) and the powder fractions marked as 1–5 with corresponding possible phases revealed with XRD. Arrows indicate the flow direction of the O_2/Ar or H_2/Ar mixture.

The outermost white layer, which was in contact with the fresh O_2/Ar gas mixture during TPOx, is mainly composed of Nb_2O_5 (Figure 5). Some lower oxides such as NbO_2 or NbO were also detected. The middle, dark layer contained mainly NbO (Figure 5) and traces of lower oxides. The lowest layer was dark grey and was also composed of NbO but

with some amount of unoxidized niobium powder. In the middle and in the lowest layer, Nb_6O was also detected. Nb_6O is a nonstoichiometric niobium oxide.

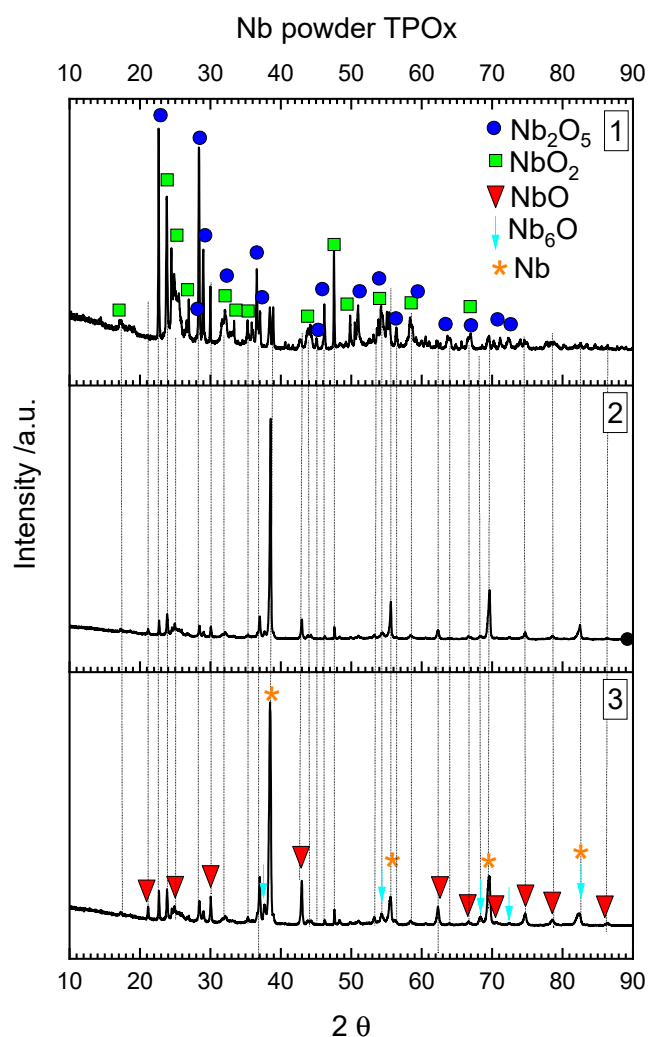


Figure 5. XRD diffraction pattern from the Nb powder after TPOx (the numbers in the upper right corner are related to the powder fractions marked in Figure 4).

In the literature between Nb and NbO, three metastable niobium oxides were described and were classified as NbO_x , NbO_{y+z} , and NbO_z . NbO_x with a stoichiometry equivalent to Nb_6O was reported to be formed at 270–530 °C. NbO_y with stoichiometry equivalent to Nb_4O was created at 330–500 °C and NbO_z with unknown stoichiometry was formed at 400–700 °C [48]. Nb_6O was also detected in a scale formed during the annealing of $\text{Nb}_{40}\text{Ti}_{30}\text{Ni}_{30}$ alloy in air at elevated-temperature [49]. The other authors claim that the first crystalline phase formed during the niobium oxidation is Nb_6O ; however, the earlier appearance of the amorphous phase hinders the formation of this oxide [50]. Niobium oxides are also considered as catalysts for hydrogen adsorption or desorption processes. Hanada et al. [51] claimed that NbO instead of Nb_2O_5 is responsible for the catalytic activity of niobium oxides and, moreover, Takahashi et al. [52] confirmed this effect on the basis of the DFT study.

In the TPOx experiment presented here, all possible niobium oxides were recognized with increasing oxygen content in the upper layer direction which was in contact with the oxygen-rich gas.

As can be seen in the TPR line in Figure 1b, the Nb powder was reduced from approximately 360 °C, close to the temperature at which the main effect of Ti reduction

also started. The shape of the TPR profile indicates that the reduction was gradual and, therefore, was most likely related to the reduction of several oxide species. It is also visible that the reduction of niobium oxides is not very intense. The measurement presented in [53] made by the temperature-programmed reduction method, carried out at a heating rate of 10deg/min, indicates that the reduction of Nb_2O_5 starts at about 350 °C, while the maximum reaches around 800 °C which is in accordance with our results.

After reduction (followed by the oxidation process) the two main powder layers are visible in the digital picture of reactor in Figure 4b. Both layers were analyzed separately with XRD (Figure 6). As follows from Figure 6, the upper layer was the most reduced (this layer was in contact with fresh H_2/Ar mixture) and composed with NbO_2 and NbO and some amount of metallic niobium powder. The underneath powder layer still contained the highest niobium oxide (Nb_2O_5), which was not reduced, probably due to the insufficient amount of hydrogen in the gas mixture. It is also difficult to recognize which of the lower niobium oxides were produced during reduction (TPR), and which of them remained after incomplete oxidation. The results presented here confirmed that reduction of Nb_2O_5 into the metallic niobium is not an easy process and probably requires stronger reducing atmospheres, as was mentioned in the introduction part. On the basis of the presented results, it could be seen that the oxidation and reduction of niobium are complex phenomena. Further investigations are planned to better understand the mechanisms of niobium oxidation and reduction.

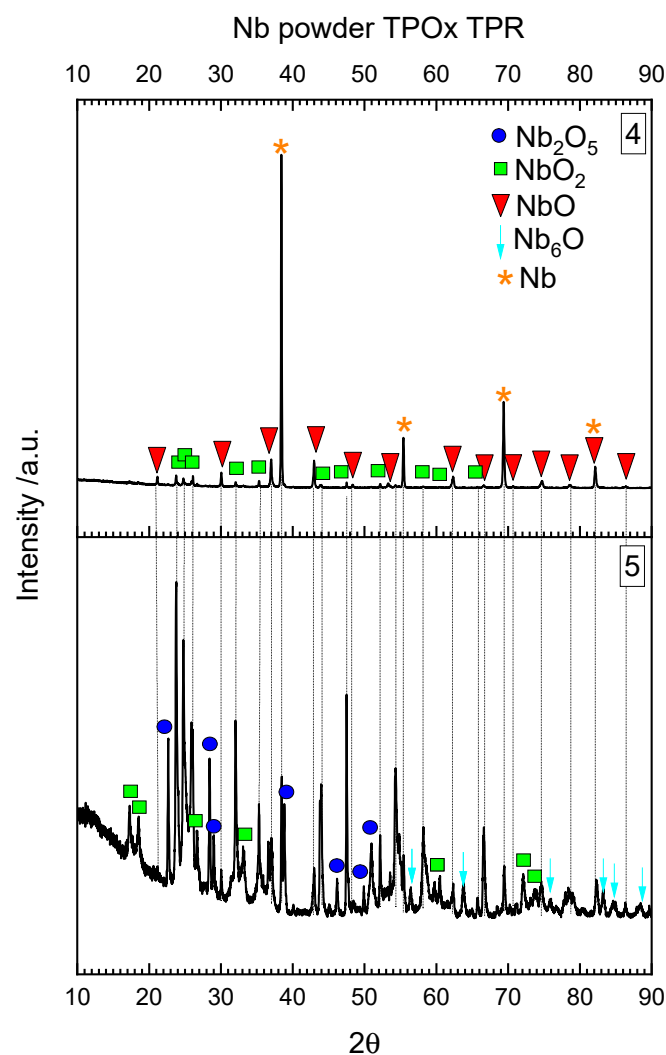


Figure 6. XRD diffraction pattern from the Nb powder after TPOx and TPR (numbers in the upper right corner are related to the powder fractions marked in Figure 4).

3.2. Oxidation and Reduction of Solid Samples

TPOx and TPR profiles (Figure 7) of solid samples are the basis for considerations regarding corrosion processes (in an atmosphere containing oxygen and containing hydrogen) of the tested metals and their alloys. Figure 7 clearly shows that both the oxidation and reduction processes, in the case of all tested materials in the form of solid samples, took place at a higher-temperature than for proper powder materials. The TPOx profiles indicate that the Ti sample oxidized at the lowest-temperature (the beginning around 320 °C, but the main oxidation at 720 °C), the next was the Nb sample (beginning at 520 °C), and only the Al sample in the all-controlled temperature-range did not oxidize. Moreover, in the case of the aluminum sample, the oxygen-releasing effect that most likely occurred on the powder material, was not observed. It can be suspected that this is the result of the small surface area of the solid sample compared to the area of powder, and, thus, the effect related to the formation and decomposition of the OAlO complex is imperceptible. Importantly, the Ti–Al alloy at the tested temperature-range did not undergo the oxidation process, which proves that this material was much more resistant to oxygen corrosion compared to pure titanium. The TPR of the Ti–Al alloy profile does not indicate any effects of hydrogen consumption, which additionally confirms that the material was resistant to high-temperature corrosion in the presence of oxygen. In order to check the influence of niobium on the Ti–Al corrosion behavior, Ti–Al–Nb solid sample was also investigated. As mentioned in the introduction, an increase in corrosion resistance was expected. As can be seen in TPOx and TPR profiles, similarly to the Ti–Al alloy, the Ti–Al–Nb material exhibited high resistance to high-temperature oxygen and hydrogen corrosion.

However, the result of diffraction analysis carried out for solids (after oxidation, and reduction) indicates that their compositions change in relation to the compositions of the starting materials, even if the TPOx/TPR profiles do not indicate the occurrence of the reaction.

As can be seen from the diffraction pattern in Figure 8a, the oxidation of the titanium sample was slightly different than the oxidation of the titanium powder. At the surface of oxidized sample only $\text{Ti}_{0.936}\text{O}_2$ rutile phase was detected. According to the literature $\text{Ti}_{0.936}\text{O}_2$ (anatase) has very good photocatalytic performance [54]. This phase was also detected on the surface of Ti–6Al–4V after electrochemical corrosion test in the LiF–NaF–KF molten salts mixture at 550 °C [55]. In Figure 8b, XRD analysis for Ti sample after oxidation and scale spallation is presented. The wide reflex between 40 and 50° probably indicated some lower oxides, e.g., TiO under the thick $\text{Ti}_{0.936}\text{O}_2$ layer. In contrast to Ti powder reduction, the composition of the solid sample after TPR was more complex, probably due to incomplete reduction. As can be seen in (Figure 8c), the TiO_2 residues are accompanied with two lower oxides: TiO and Ti_3O_5 . Moreover, some very small amount of undecomposed TiH_2 was also identified with XRD analysis.

In comparison to the composition of powder after reduction (Figure 3), the titanium sample reduced to a lesser extent. It is also possible that the detected TiO and Ti_3O_5 oxides were present before reduction after oxidation beneath TiO_2 and was exposed after TiO_2 spallation. TiO_2 spallation was caused by the temperature changes during cooling and heating between TPOx and TPR measurement. It is well known that the thermal expansion coefficients for titanium and TiO_2 (rutile) are different and equal, respectively: $8.5 \cdot 10^{-6}/\text{deg}$ (at RT) and depending on the rutile unit cell crystallographic axes $a = 6.99953 \cdot 10^{-6}/\text{deg}$, $c = 9.36625 \cdot 10^{-6}/\text{deg}$, and $= 28.680 \cdot 10^{-6}/\text{deg}$, which can promote scale spallation under thermal cycling conditions [56,57]. This hypothesis is also in agreement with the morphology of scale formed on titanium after oxidation described in the introduction part and with the microscopic observations of titanium cross-section and scale after oxidation presented in Figure 9a–c. As it is visible the spalled scale was rather thick with a well-crystallized rutile phase. The thickness of the oxide layer remaining on the surface was about 1.5 μm .

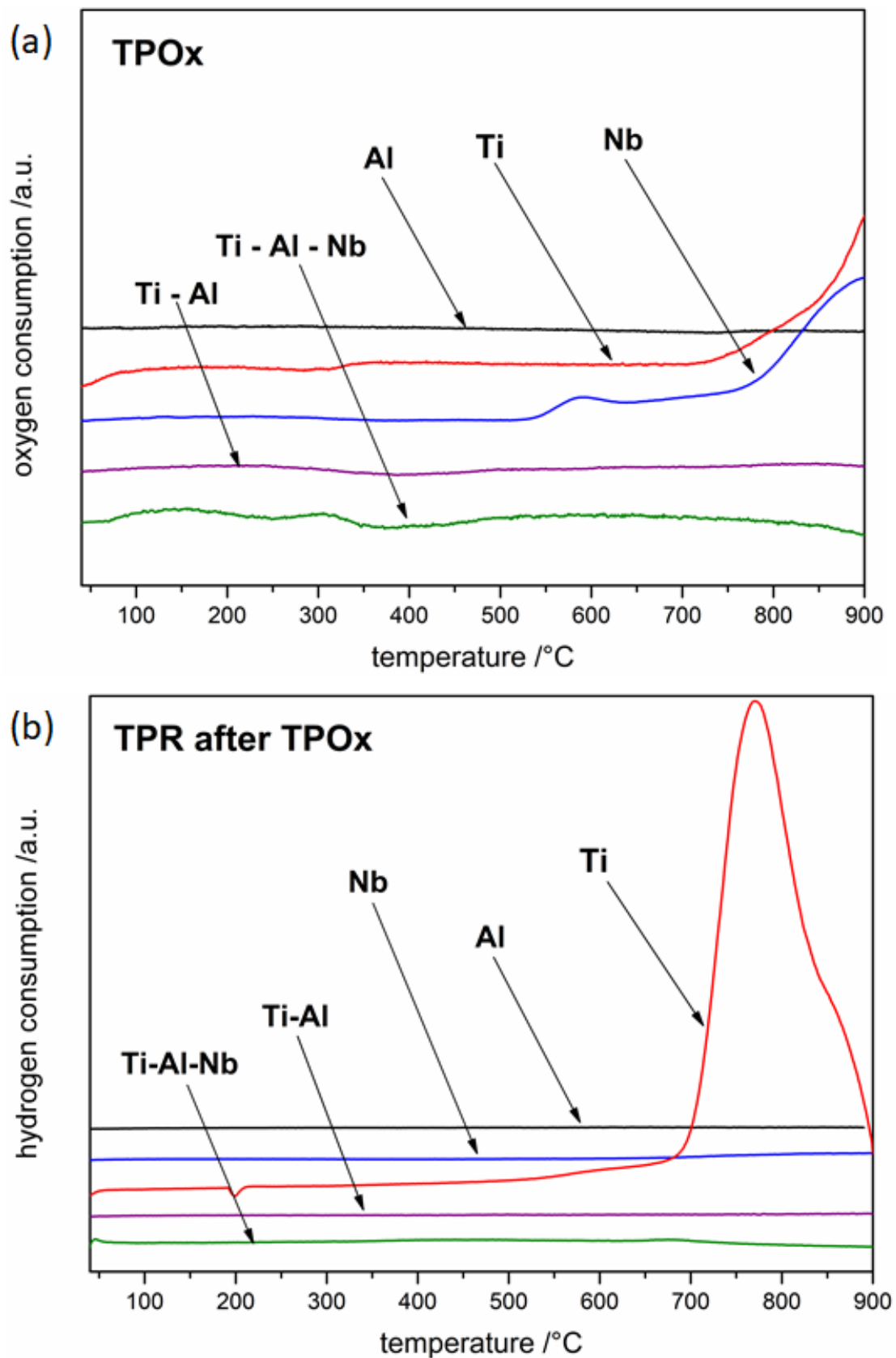


Figure 7. The oxidation (a) and reduction (b) profiles of tested solid samples.

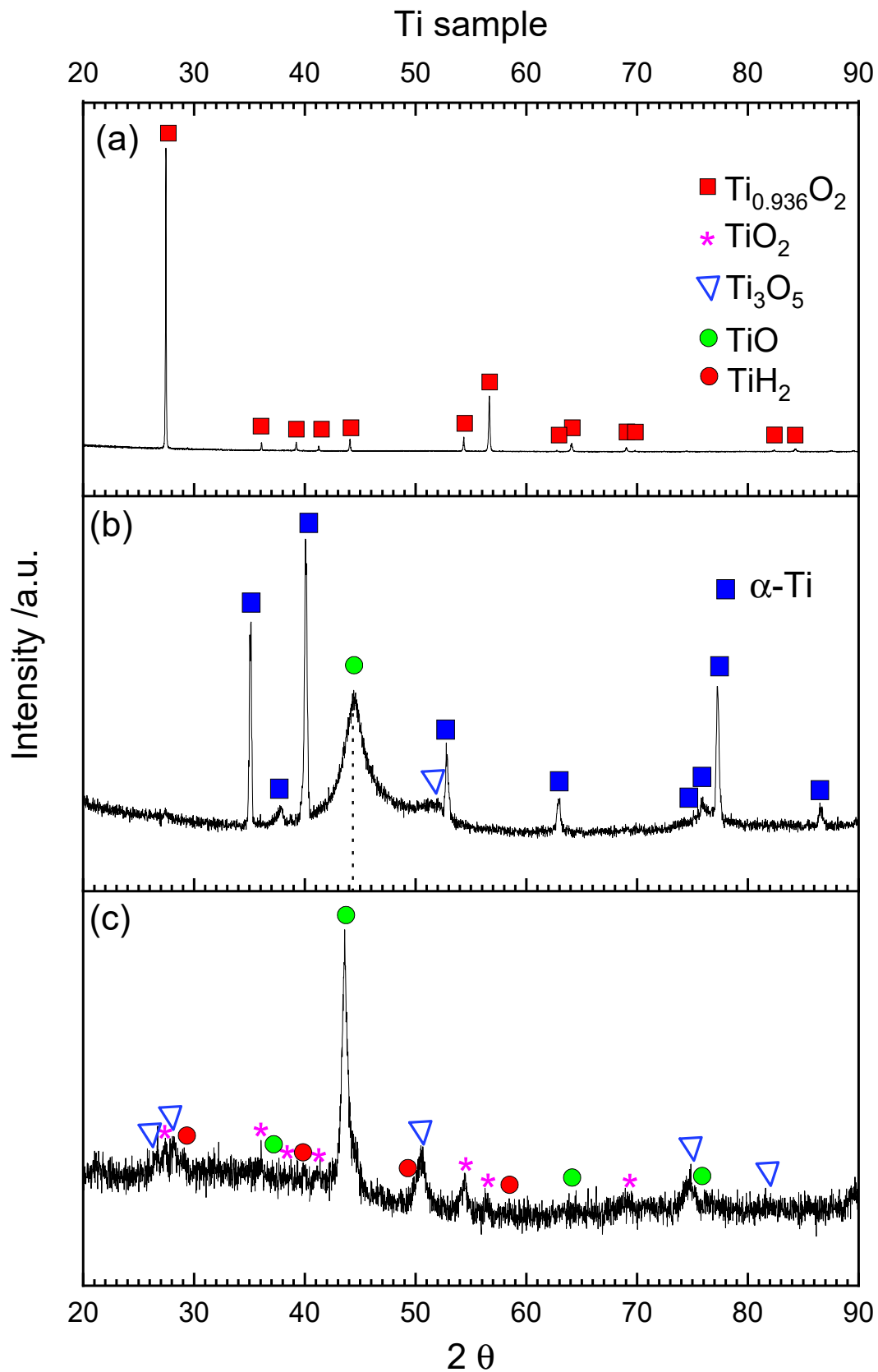


Figure 8. XRD diffraction pattern of the Ti solid sample after TPOx (spalled scale (a), sample surface below the scale, XRD-GID (b)) and TPOx + TPR (surface of sample, XRD-GID (c)).

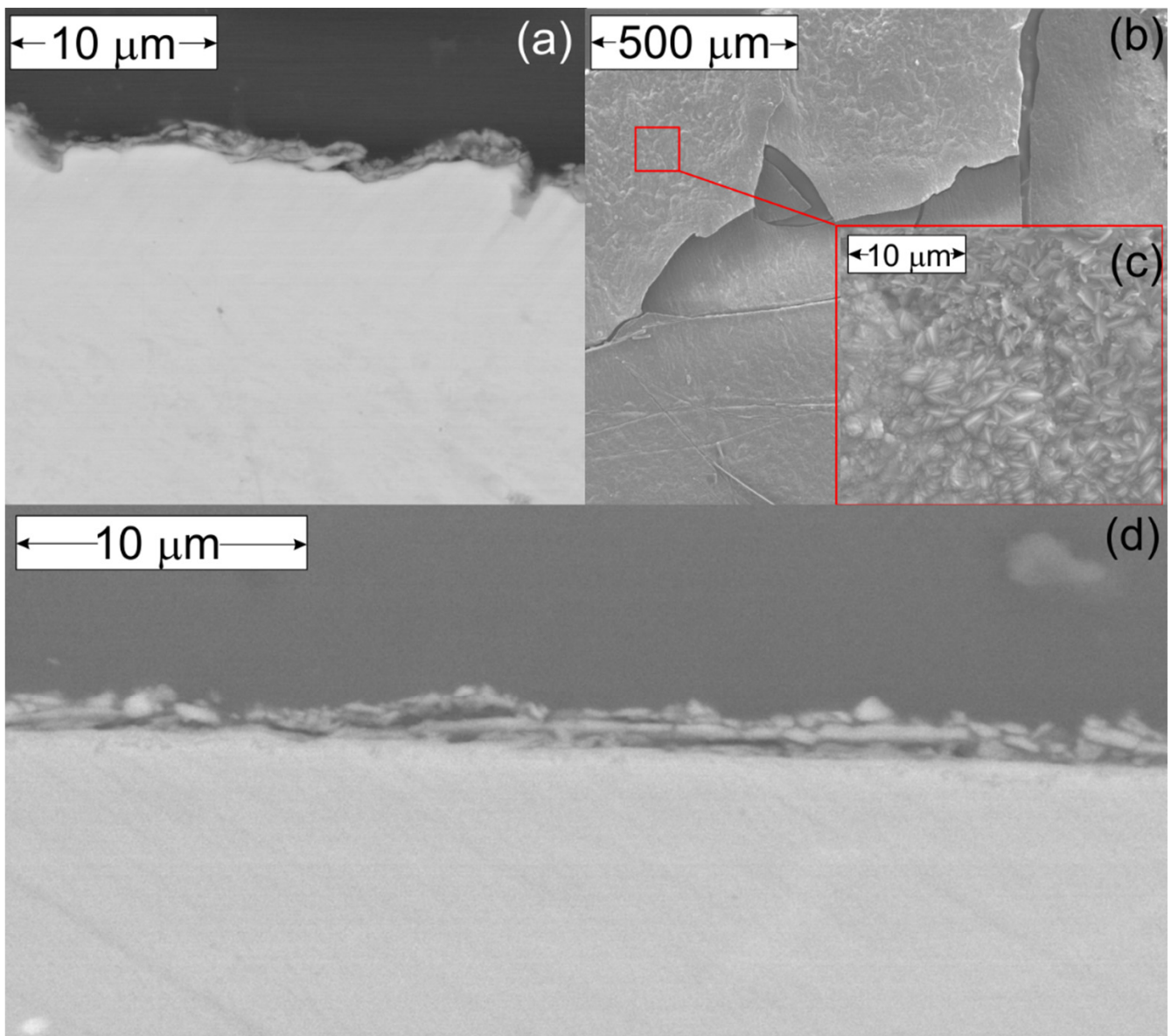


Figure 9. BE image of Ti sample cross-section after TPOx without the spalled scale (a) and SE image of the spalled scale (b) with visible rutile crystals in the higher-magnification frame (c). BE image of Ti–Al–Nb sample cross-section after TPOx + TPR (d).

XRD results for the Ti–Al sample are shown in Figure 10a. The broad peaks indicate the presence of amorphous phase, probably Al_2O_3 . Some reflexes can be identified as $\text{-Al}_2\text{O}_3$ (with exact stoichiometry $\text{Al}_{2.666}\text{O}_{3.999}$). The main alloy phase (TiAl) can also be recognized. After reduction the amount of aluminum oxide is lower and some reflexes from the Ti–Al phase became more visible (Figure 10b). These results are not in accordance with the literature, because thermodynamical calculations showed that for titanium aluminides, containing about 50 at.% aluminum or less, titanium oxide rather than aluminum oxide was the stable phase [58]. In other articles, it was found that approximately 60–70% of aluminum is needed for Ti–Al alloys to form a continuous layer of Al_2O_3 during oxidation in air and approximately 47–49% of aluminum is needed during oxidation in pure oxygen [59–61].

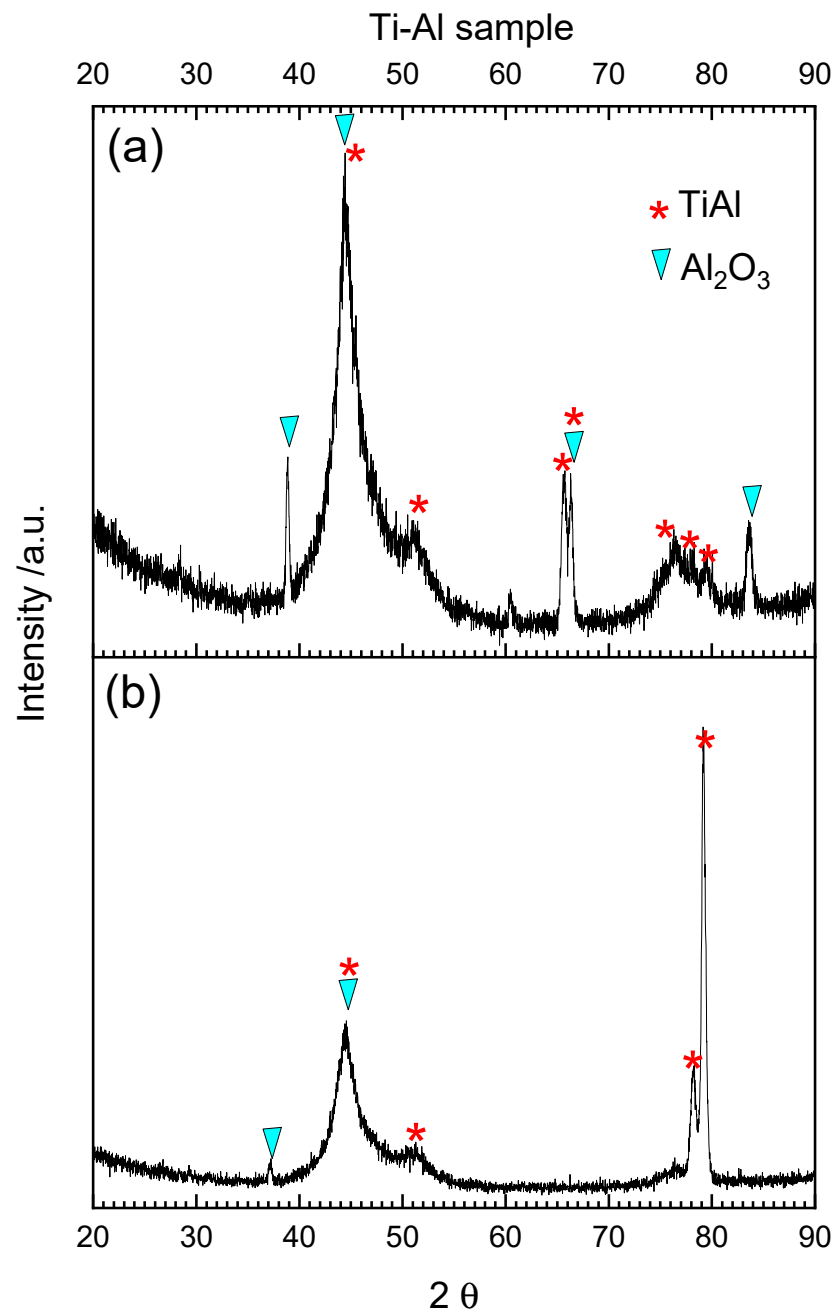


Figure 10. XRD-GID diffraction pattern from the Ti–Al solid sample after TPOx (a) and TPOx + TPR (b).

The composition of the scale formed on the niobium sample after oxidation is very simple and the highest oxide was mainly detected (Figure 11a). Niobium has a high affinity for oxygen and can very easily create Nb₂O₅ oxide. The presence of lower niobium oxides is possible only when the insufficient amount of oxygen is used [62]. It is also possible that beneath Nb₂O₅ in the oxide/metal interface some lower Nb oxides were present, as visible in Figure 11a NbO₂ and NbO. After reduction (Figure 11b) the scale was built mainly with niobium dioxide (NbO₂) probably from Nb₂O₅ reduction and with a smaller amount of Nb₂O₅ and NbO. Oxidation and reduction of a solid sample similar to titanium is different than for powder. In the case of powder, the surface in contact with the oxidizing/reducing agent is large and the oxidation/reduction is faster, limited only by the availability of the reactant. In the case of solid samples, the surface is relatively small and the products created at the surface can behave as a diffusion barrier for further oxidation/reduction.

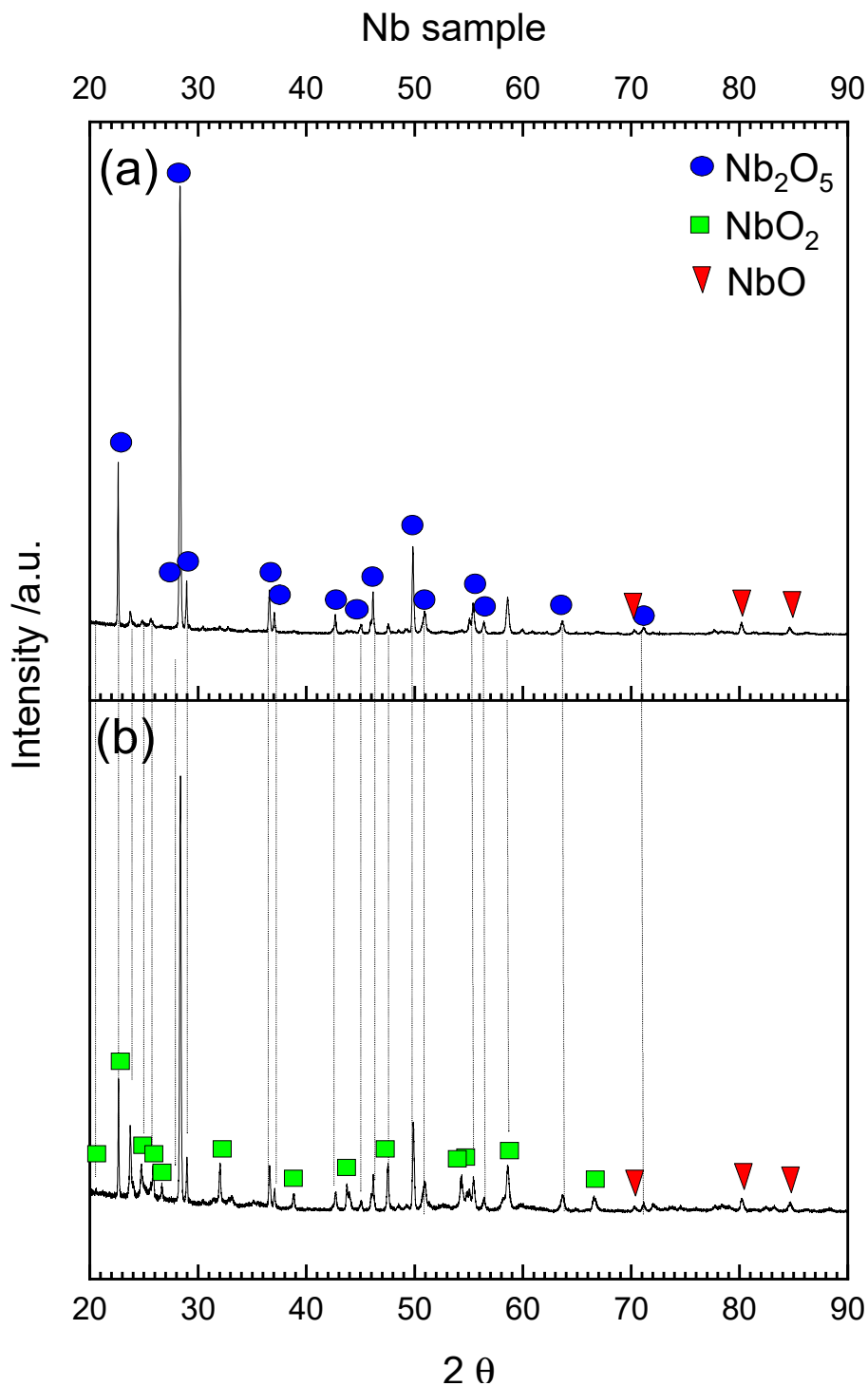


Figure 11. XRD diffraction pattern from the Nb solid sample spalled scale after TPOx (a) and TPOx + TPR (b).

Interpretation of XRD results for Ti–Al–Nb sample after oxidation and reduction is difficult because many reflexes overlapped. As can be seen in the XRD pattern in Figure 12a after oxidation only two phases are clearly visible: TiAl (substrate) and TiO_2 (rutile). However, the presence of small amount of Al_2O_3 was also possible, because some reflexes of TiAl and Al_2O_3 phases overlapped. The presence of the second substrate alloy phase-Ti₃Al after oxidation was not confirmed with XRD but it is not excluded because reflexes from this phase overlapped with those from TiO_2 . According to the literature at the

beginning of oxidation, oxygen dissolves in the alloy and the amount of dissolved oxygen depends on the TiAl phase and is equal: 16 at.% for α_2 -Ti₃Al and 2 at.% for TiAl [63]. Next ultrathin layer of alumina is formed (about two times thicker for α_2 -Ti₃Al) which results in Al-depletion in metallic phase. When the critical concentration of aluminum is reached, titanium oxidation occurs and TiO₂ is formed on the surface.

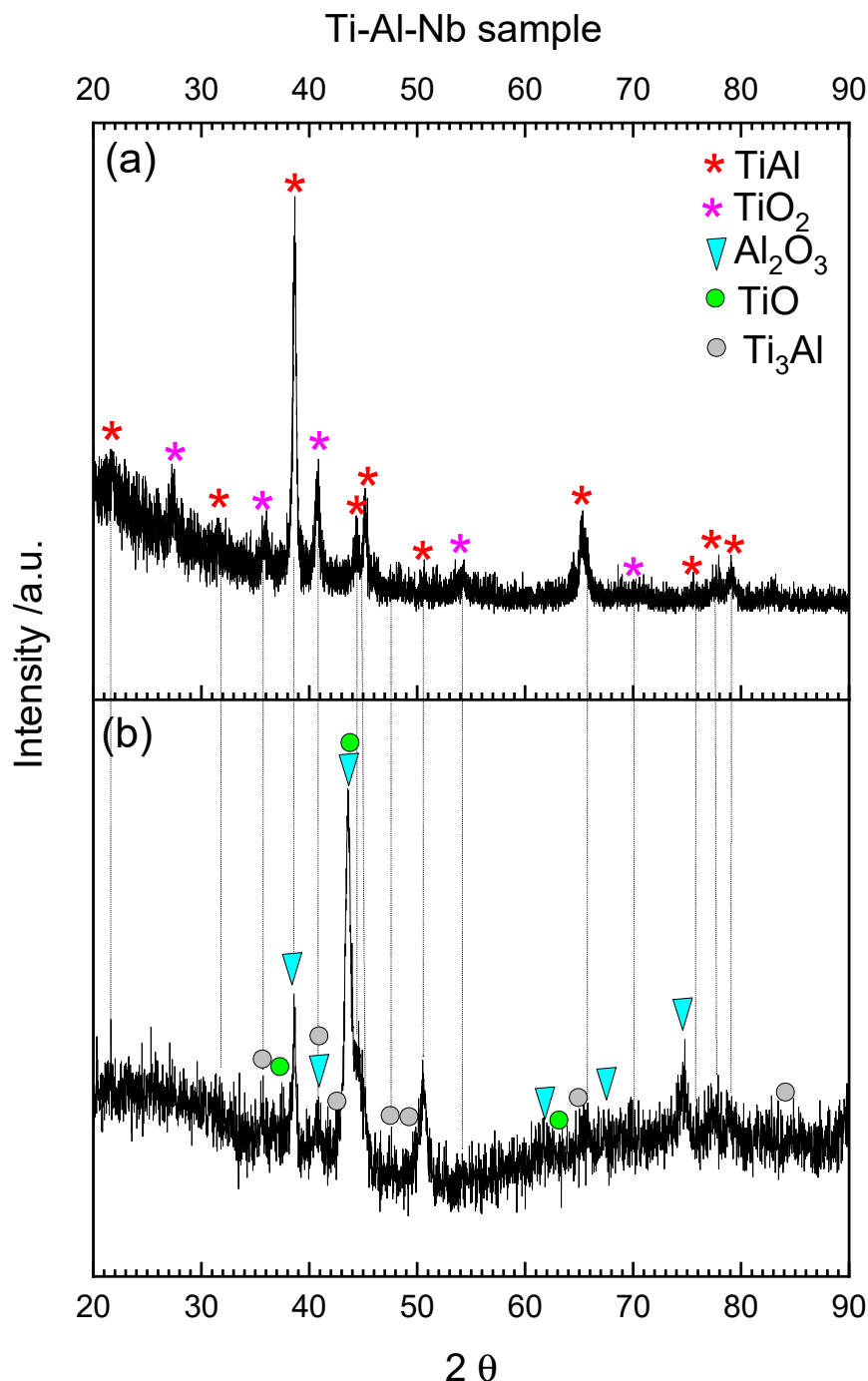


Figure 12. XRD-GID diffraction pattern from the Ti-Al-Nb solid sample after TPOx (a) and TPOx + TPR (b).

According to the diffraction pattern in Figure 12b after TPR, the outermost layer of TiO₂ was reduced to TiO. The inner layer of Al₂O₃ became more visible and was not completely reduced. Reflexes from the Ti₃Al phase were easier to identify in the XRD

pattern after reduction. The presence of very thin (around 0.5 μm) remaining oxide scale after TPR was confirmed with microscopic observations shown in Figure 9d.

Note that in the case of all tested solid samples, both the phase composition (XRD) and the observations with SEM give more information than the TPOx/TPR method, which was definitely more useful in the case of powder samples.

4. Conclusions

Titanium aluminides are interesting for structural applications in transportation, because they have low density, high strength, and promising resistance to oxidation at moderate-temperatures. Therefore, in-depth analysis of the oxidation and reduction processes of alloys is particularly important in the context of their resistance to the oxidizing and reducing atmosphere. The oxidation and reduction of powder materials based on the Ti–Al system are also important for catalytic applications, because titanium and aluminum oxides are often used as supports for catalytically active metals in redox reactions. Additionally, some authors consider niobium oxides as catalysts for hydrogen adsorption or desorption processes.

The mechanisms of Al, Ti, Nb, Ti–Al, and Ti–Al–Nb oxidation and subsequent reduction were different for powders and solid samples what was confirmed by TPOx/TPR profiles, as well as by phase composition analysis and microscopy observations after oxidation and reduction processes. In the next experiments it is planned to recognize if the differences between oxidation and reduction of powders and solids are kinetic or thermodynamic in nature. Further investigations are also necessary to specify the exact mechanism for Ti–Al–Nb alloy oxidation. Especially understanding of the alloy reduction may be of great importance in the context of its predicted application in the aerospace or automotive industry (construction of valves, turbocharger rotors, and components of exhaust systems), where hydrogen fuel is the future.

The TPOx results showed that the Ti–Al sample is more resistant to oxidation than titanium and aluminum separately, both for powder materials and solid samples. The oxidation of Ti–Al is often described in the literature as a two-stage process, whereas hereby three stages of oxidation were revealed: the first stage was the formation and decomposition of the OAlO complex, the next creation of amorphous Al_2O_3 , followed by the growth of TiO_2 .

It seems that the introduction of niobium into the Ti–Al system changed the mechanism of Ti–Al–Nb alloy oxidation. Interestingly, in the case of Ti–Al–Nb oxidation, TiO_2 was the predominant phase, while alumina was probably only in the amorphous form. This result is in contradiction to the beneficial effect of niobium in alumina formation described in the literature. Detailed explanation of the influence of niobium on the oxidation, as well as the reduction of the Ti–Al–Nb alloy is planned in the future. Well-controlled TPOx/TPR conditions and in situ XRD measurement are considered.

The factor significantly affecting the usefulness of the TPOx/TPR method is the specific surface area of the tested materials; in the case of powder materials, the sensitivity of these methods was greater than that of the X-ray diffraction method, hence its use to study the reaction mechanism was fully justified. It was different in the case of testing solid materials, when this method was definitely less useful due to small specific surfaces of the samples. Moreover, TPOx/TPR allows to investigate only relatively short-term processes.

Author Contributions: Methodology, M.M.-K. and E.D.; investigation, M.M.-K. and E.D.; writing—original draft preparation, M.M.-K. and E.D.; writing—review and editing, M.M.-K. and E.D.; visualization, M.M.-K. All authors have read and agreed to the published version of the manuscript.

Funding: This work was supported from the subsidy of the Ministry of Education and Science for the AGH University of Science and Technology in Kraków (Project No 16.16.160.557).

Institutional Review Board Statement: Not applicable.

Informed Consent Statement: Not applicable.

Data Availability Statement: Data will be made available upon reasonable request.

Acknowledgments: The authors acknowledge contribution of Bartosz Handke from the Faculty of Materials Science and Ceramics, AGH UST, who was involved in the XRD measurement.

Conflicts of Interest: The authors declare no conflict of interest.

References

1. Lu, G.; Bernasek, S.L.; Schwartz, J.V. Oxidation of a polycrystalline titanium surface by oxygen and water. *Surf. Sci.* **2000**, *458*, 80–90. [[CrossRef](#)]
2. Vaquila, I.; Vergara, L.I.; Passeggi, M.C.G., Jr.; Vidal, R.A.; Ferrón, J. Chemical reactions at surfaces: Titanium oxidation. *Surf. Coat. Tech.* **1999**, *122*, 67–71. [[CrossRef](#)]
3. Okamoto, H. O-Ti (Oxygen-Titanium). *J. Phase Equilib. Diffus.* **2011**, *32*, 473–474. [[CrossRef](#)]
4. Unnam, J.; Shenoy, R.N.; Clark, R.K. Oxidation of Commercial Purity Titanium. *Oxid. Met.* **1986**, *26*, 231–252. [[CrossRef](#)]
5. Kofstad, P.; Haufler, K. Oxidation von Titan. *Werkst. Korros.* **1956**, *11*, 642–649. [[CrossRef](#)]
6. Kofstad, P. High-temperature oxidation of titanium. *J. Less Common Met.* **1967**, *12*, 449–464. [[CrossRef](#)]
7. NIST Chemistry WebBook. Available online: <https://webbook.nist.gov/chemistry/> (accessed on 9 November 2021).
8. Marshall, P.; O'Connor, P.B.; Chan, W.-T.; Kristof, P.V.; Goddard, J.D. Reactions of boron and aluminum atoms with small molecules. In *Gas Phase Metal Reactions*; Fontijn, A., Ed.; Elsevier Science Publishers B.V.: North Holland, Netherlands, 1992; pp. 147–177.
9. Garland, N.L. Kinetic Studies of Boron and Aluminum Species. In *Gas Phase Metal Reactions*; Fontijn, A., Ed.; Elsevier Science Publishers B.V.: North Holland, The Netherlands, 1992; pp. 73–91.
10. Vorozhtsov, A.B.; Lerner, M.; Rodkevich, N.; Nie, H.; Abraham, A.; Schoenitz, M.; Dreizin, E.L. Oxidation of nano-sized aluminum powders. *Thermochim. Acta* **2016**, *636*, 48–56. [[CrossRef](#)]
11. Nico, C.; Monteiro, T.; Graça, M.P.F. Niobium oxides and niobates physical properties: Review and prospects. *Prog. Mater. Sci.* **2016**, *80*, 1–37. [[CrossRef](#)]
12. Delheusy, M.; Stierle, A.; Kasper, N.; Kurta, R.P.; Vlad, A.; Dosch, H.; Antoine, C.; Resta, A.; Lundgren, E.; Andersen, J. X-ray investigation of subsurface interstitial oxygen at Nb/oxide interfaces. *Appl. Phys. Lett.* **2008**, *92*, 1–3. [[CrossRef](#)]
13. Nico, C.; Rino, L.; Mtos, M.; Monteiro, M.; Costa, F.M.; Monteiro, T.; Graça, M.P.F. NbO/Nb₂O₅ core-shells by thermal oxidations. *J. Eur. Ceram. Soc.* **2013**, *33*, 15–16. [[CrossRef](#)]
14. Newbery, E.; Pring, J.N. The reduction of metallic oxides with hydrogen at high pressures. *Proc. R. Soc. Lond. A* **1916**, *639*, 276–285. [[CrossRef](#)]
15. Rojas, E.; Delgado, J.J.; Guerrero-Pérez, M.O.; Bañares, M.A. Performance of NiO and Ni–Nb–O active phases during the ethane ammoxidation into acetonitrile. *Catal. Sci. Technol.* **2013**, *3*, 3173–3182. [[CrossRef](#)]
16. Appel, F.; Wagner, R. Microstructure and deformation of two-phase γ -Titanium Aluminides. *Mater. Sci. Eng. R.* **1998**, *5*, 187–268. [[CrossRef](#)]
17. Voice, W.E.; Henderson, M.; Shelton, E.F.J.; Wu, X. Gamma titanium aluminide, TNB. *Intermetallics* **2005**, *9*, 959–964. [[CrossRef](#)]
18. Mitoraj, M.; Godlewska, E.; Heintz, O.; Geoffroy, N.; Fontana, S.; Chevalier, S. Scale composition and oxidation mechanism of the Ti-46Al-8Nb alloy in air at 700 and 800 °C. *Intermetallics* **2011**, *1*, 39–47. [[CrossRef](#)]
19. Yue, X.; Shen, J.; Xiong, Y.; Li, Q.; Zheng, S. Microstructure, fracture toughness and high-temperature tensile property of large size Ti-46Al-5Nb-0.18C-0.3Si alloy with oriented lamella by electromagnetic confinement directional solidification. *Mat. Sci. Eng. A* **2021**, *812*, 141139. [[CrossRef](#)]
20. Ibáñez-Pérez, J.; Nób, M.L.; Oehring, M.; Clemens, H.; San Juan, J.M. Influence of Nb on Ti diffusion in γ -TiAl intermetallics studied by mechanical spectroscopy. *J. Alloys Compd.* **2021**, *867*, 158880. [[CrossRef](#)]
21. Lin, J.P.; Zhao, L.L.; Li, G.Y.; Zhang, L.Q.; Song, X.P.; Ye, F.; Chen, G.L. Effect of Nb on oxidation behavior of high Nb containing TiAl alloys. *Intermetallics* **2011**, *2*, 131–136. [[CrossRef](#)]
22. Cui, Y.; Aoyagi, K.; Koizumi, Y.; Yang, C.; Bian, H.; Hayasaka, Y.; Fujieda, T.; Chiba, A. Effect of niobium addition on tensile properties and oxidation resistance of a titanium-based alloy. *Corros. Sci.* **2021**, *180*, 109198. [[CrossRef](#)]
23. Pan, D.; Ru, Y.; Liu, T.; Wang, Y.; Yu, F.; Chen, S.; Yan, X.; Fan, B.; Li, R. Highly efficient and stable ordered mesoporous Ti-Al composite oxide catalyst for oxidative dehydrogenation of ethylbenzene to styrene with CO₂. *Chem. Eng. Sci.* **2022**, *15*, 117388. [[CrossRef](#)]
24. Jostons, A.; Malin, A.S. The ordered structure of Ti₃O. *Acta Cryst.* **1968**, *2*, 211–213. [[CrossRef](#)]
25. Peng, W.; Zeng, W.; Zhang, Y.; Shi, C.; Quan, B.; Wu, J. The Effect of Colored Titanium Oxides on the Color Change on the Surface of Ti-5Al-5Mo-5V-1Cr-1Fe Alloy. *J. Mater. Eng. Perform.* **2013**, *22*, 2588–2593. [[CrossRef](#)]
26. Zhu, Q.; Peng, Y.; Lin, L.; Fan, C.-M.; Gao, G.-Q.; Wang, R.-X.; Xu, A.-W. Stable blue TiO_{2-x} nanoparticles for efficient visible light photocatalysts. *J. Mater. Chem. A* **2014**, *2*, 4429–4437. [[CrossRef](#)]
27. Qiu, J.; Li, S.; Gray, E.; Liu, H.; Gu, Q.-F.; Sun, C.; Lai, C.; Zhao, H.; Zhang, S. Hydrogenation Synthesis of Blue TiO₂ for High-Performance Lithium-Ion Batteries. *J. Phys. Chem. C* **2014**, *118*, 8824–8830. [[CrossRef](#)]
28. Kong, L.; Wang, C.; Zheng, H.; Zhang, X.; Liu, Y. Defect-Induced Yellow Color in Nb-Doped TiO₂ and Its Impact on Visible-Light Photocatalysis. *J. Phys. Chem. C* **2015**, *119*, 16623–16632. [[CrossRef](#)]

29. Wu, Q.; Huang, F.; Zhao, M.; Xua, J.; Zhou, J.; Wang, Y. Ultra-small yellow defective TiO₂ nanoparticles for co-catalyst free photocatalytic hydrogen production. *Nano Energy* **2016**, *24*, 63–71. [[CrossRef](#)]
30. Li, Y.; Yang, Y.; Shu, X.; Wan, D.; Wei, N.; Yu, X.; Breese, M.B.H.; Venkatesan, T.; Xue, J.M.; Liu, Y.; et al. From Titanium Sesquioxide to Titanium Dioxide: Oxidation-Induced Structural, Phase, and Property Evolution. *Chem. Mater.* **2018**, *13*, 4383–4392. [[CrossRef](#)]
31. Khader, M.M.; Kheiri, F.M.-N.; El-Anadouli, B.E.; Ateya, B.G. Mechanism of Reduction of Rutile with Hydrogen. *J. Phys. Chem.* **1993**, *97*, 6074–6077. [[CrossRef](#)]
32. Bratan, V.; Munteanu, C.; Hornoiu, C.; Vasile, A.; Papa, F.; State, R.; Preda, S.; Culita, D.; Ionescu, N.I. CO oxidation over Pd supported catalysts —In situ study of the electric and catalytic properties. *Appl. Catal. B-Environ.* **2017**, *207*, 166–173. [[CrossRef](#)]
33. Zhang, W.; Sadedin, D.R.; Reuter, M.A.; McCallum, J.C. The de-oxidation of partially oxidized titanium by hydrogen plasma. *Mater. Forum* **2007**, *31*, 76–83.
34. Lindemann, I.; Herrich, M.; Gebel, B.; Schmidt, R.; Stoeck, U.; Uhlemann, M.; Gebert, A. Synthesis of spherical nanocrystalline titanium hydride powder via calciothermic low temperature reduction. *Scripta Mater.* **2017**, *130*, 256–259. [[CrossRef](#)]
35. Murray, J.L.; Wriedt, H.A. The O-Ti (Oxygen-Titanium) System. *J. Phase Equilib.* **1987**, *8*, 148–165. [[CrossRef](#)]
36. Williams, D.N.; Koehl, B.G.; Bartlett, E.S. The reaction of titanium with hydrogen gas at ambient temperatures. *J. Less-Common Met.* **1969**, *4*, 385–398. [[CrossRef](#)]
37. Jeurgens, L.P.H.; Sloof, W.G.; Tichelaar, F.D.; Mittemeijer, E.J. Thermodynamic stability of amorphous oxide films on metals: Application to aluminum oxide films on aluminum substrates. *Phys. Rev. B* **2000**, *62*, 4707–4719. [[CrossRef](#)]
38. Jeurgens, L.P.H.; Sloof, W.G.; Tichelaar, F.D.; Mittemeijer, J. Structure and morphology of aluminium-oxide films formed by thermal oxidation of aluminium. *Thin Solid Film* **2002**, *418*, 89–101. [[CrossRef](#)]
39. Hoivik, N.D.; Elam, J.W.; Linderman, R.J.; Bright, V.M.; George, S.M.; Lee, Y.C. Atomic layer deposited protective coatings for micro-electromechanical systems. *Sens. Actuators A* **2003**, *1–2*, 100–108. [[CrossRef](#)]
40. Sanchez-Lopez, J.C.; Gonzalez-Elipse, A.R.; Fernandez, A. Passivation of Nano Crystalline Al Prepared by the Gas. *J. Mater. Res.* **1998**, *3*, 703–707. [[CrossRef](#)]
41. Reichel, F.; Jeurgens, L.P.H.; Richter, G.; Mittemeijer, E.J. Amorphous versus crystalline state for ultrathin Al₂O₃ overgrowths on Al Substrates. *J. Appl. Phys.* **2008**, *103*, 1–10. [[CrossRef](#)]
42. Trunov, M.A.; Schoenitz, M.; Zhu, X.; Dreizin, E.L. Effect of polymorphic phase transformations in Al₂O₃ film on oxidation kinetics of aluminum powders. *Combust. Flame* **2005**, *4*, 310–318. [[CrossRef](#)]
43. Hasani, S.; Panjepour, M.; Shamanian, M. The Oxidation Mechanism of Pure Aluminum Powder Particles. *Oxid. Met.* **2012**, *3*, 179–195. [[CrossRef](#)]
44. Barin, I.; Knacke, O. *Thermochemical Properties of Inorganic Substances*; Springer: Berlin, Germany, 1973; pp. 11, 29, 30–32, 316, 323.
45. Braaten, O.; Kjekshus, A.; Kvande, H. The Possible Reduction of Alumina to Aluminum Using Hydrogen. *JOM* **2000**, *52*, 47–53. [[CrossRef](#)]
46. Talbot, D.E.J.; Anyalebechi, P.N. Solubility of hydrogen in liquid aluminium. *Mater. Sci. Tech.* **1988**, *1*, 1–4. [[CrossRef](#)]
47. Weller, S.W.; Montagna, A.A. Studies of alumina I. Reaction with hydrogen at elevated temperatures. *J. Catalysis* **1971**, *3*, 303–311. [[CrossRef](#)]
48. Niebuhr, J. Die niederen Oxide des Niobs. *J. Less Common Met.* **1966**, *11*, 191–203. [[CrossRef](#)]
49. Ishikawa, K.; Habaguchi, H.; Obata, N.; Kobori, Y.; Ohtsu, N.; Aoki, K. Formation of surface oxides and its effects on the hydrogen permeability of Nb₄₀Ti₃₀Ni₃₀ alloy. *Int. J. Hydrogen Energ.* **2016**, *10*, 5269–5275. [[CrossRef](#)]
50. Shamrai, V.F.; Blagoveshchenski, Y.V.; Gordeev, A.S.; Mitin, A.V.; Drobinova, I.A. Structural States and Electrical Conductivity of Oxidized Niobium Nanopowders. *Russ. Metall. Met.* **2007**, *4*, 322–326. [[CrossRef](#)]
51. Honada, N.; Ichikawa, T.; Isobe, S.; Nakagawa, T.; Tokoyoda, K.; Honma, T.; Fuji, H.; Kojima, Y. X-ray Absorption Spectroscopic Study on Valence State and Local Atomic Structure of Transition Metal Oxides Doped in MgH₂. *J. Phys. Chem. C* **2009**, *30*, 13450–13455. [[CrossRef](#)]
52. Takahashi, K.; Isobe, S.; Ohnuki, S. The catalytic effect of Nb, NbO and Nb₂O₅ with different surface planes on dehydrogenation in MgH₂: Density functional theory study. *J. Alloy. Comp.* **2013**, *1*, S25–S28. [[CrossRef](#)]
53. Batalu, D.; Coşmeleaţă, G.; Aloman, A. Critical analysis of the Ti-Al phase diagrams. *UPB Sci. Bull. B Chem. Mater. Sci.* **2006**, *68*, 77–90.
54. Pan, L.; Ai, M.; Huang, C.; Yin, L.; Liu, X.; Zhang, R.; Wang, S.; Jiang, Z.; Zhang, X.; Zou, J.-J.; et al. Manipulating spin polarization of titanium dioxide for efficient photocatalysis. *Nat. Commun.* **2020**, *418*, 1–9. [[CrossRef](#)]
55. Neacsu, E.I.; Constantin, V.; Yanushkevich, K.; Donath, C.; Anastasescu, M.; Popescu, A.M. Modification on Ti-6Al-4V Alloy During Corrosion in a High Temperature Ionic Liquid. *Rev. Chim.* **2020**, *4*, 201–219. [[CrossRef](#)]
56. Hidnert, P. Thermal expansion of titanium. *J. Res. Nat. Bur. Stand.* **1943**, *30*, 101–105. [[CrossRef](#)]
57. Hummer, D.R.; Heaney, P.J.; Post, J.E. Thermal expansion of anatase and rutile between 300 and 575 K using synchrotron powder X-ray diffraction. *Powder Diffraction* **2007**, *4*, 352–357. [[CrossRef](#)]
58. McKee, D.W.; Huang, S.-C. High Temperature Ordered Intermetallic Alloys IV. In Proceedings of the 4th MRS Symposium, Boston, MA, USA, 27–30 November 1990; Johnson, L.A., Pope, D.P., Stiegler, J.O., Eds.; Materials Research Society: Pittsburgh, PA, USA, 1991; p. 939.
59. Meier, G.H. Fundamentals of the oxidation of high-temperature intermetallics. In *Oxidation of High-Temperature Intermetallics*; Grobstein, T., Doychak, J., Eds.; The Minerals, Metals & Materials Society: Pittsburgh, PA, USA, 1988; pp. 1–17.

60. Shida, Y.; Anada, H. Oxidation Behavior of Binary TiAl Alloys in High Temperature Air Environment. *Mater. Trans. JIM* **1993**, *3*, 236–242. [[CrossRef](#)]
61. Rahmel, A.; Quadackers, W.J.; Schütze, M. Fundamentals of TiAl Oxidation—A Critical Review. *Werkst. Korros.* **1995**, *5*, 271–285. [[CrossRef](#)]
62. Oliveira, R.M.; Hoshida, L.; Oliveira, A.C.; Silva, M.M.N.F.; Pichon, L.; Santos, N.M. Evaluation of the resistance to oxidation of niobium treated by high temperature nitrogen Plasma Based Ion Implantation. *Surf. Coat. Tech.* **2017**, *312*, 110–116. [[CrossRef](#)]
63. Maurice, V.; Despert, G.; Zanna, S.; Josso, P.; Bacos, M.-P.; Marcus, P. XPS study of the initial stages of oxidation of α_2 -Ti₃Al and γ -TiAl intermetallic alloys. *Acta Mater.* **2007**, *10*, 3315–3325. [[CrossRef](#)]